Copper Sulfide Nanoparticles As a New Class of Photoacoustic Contrast Agent for Deep Tissue Imaging at 1064 nm

Geng Ku,[†,§] Min Zhou,[†,§] Shaoli Song,[†,⊥] Qian Huang,[†] John Hazle,[‡] and Chun Li[†,*]

[†]Department of Experimental Diagnostic Imaging and [‡]Imaging Physics, The University of Texas MD Anderson Cancer Center, Houston, Texas 77030, United States. [§]These authors contributed equally to this work. [⊥]Present address: Department of Nuclear Medicine, RenJi Hospital, School of Medicine, ShangHai JiaoTong University, Shanghai 200127, China.

ABSTRACT

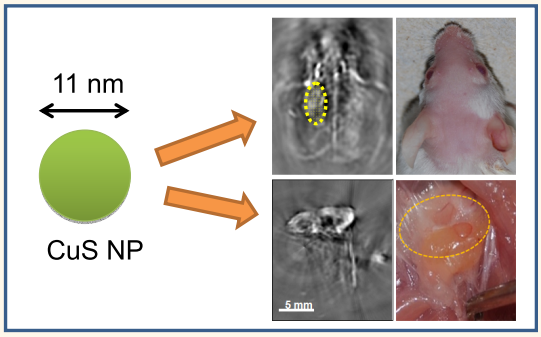

Photoacoustic tomography (PAT) is an emerging molecular imaging modality. Here, we demonstrate use of semiconductor copper sulfide nanoparticles (CuS NPs) for PAT with an Nd:YAG laser at a wavelength of 1064 nm. CuS NPs allowed visualization of mouse brain after intracranial injection, rat lymph nodes 12 mm below the skin after interstitial injection, and CuS NP-containing agarose gel embedded in chicken breast muscle at a depth of ~5 cm. This imaging approach has great potential for molecular imaging of breast cancer.

KEYWORDS: photoacoustic tomography · CuS nanoparticles · 1064 nm laser · optical imaging

Photoacoustic tomography (PAT), also referred to as optoacoustic tomography, is based on the measurement of ultrasonic waves induced by biological tissues' absorption of short laser pulses. PAT employs nonionizing laser light to acoustically visualize biological tissues with high optical contrast and high ultrasonic resolution. Photoacoustic effects were demonstrated in turbid medium by Kruger[1] in 1994, in biological tissues by Oraevsky *et al.*[2] in 1997, and in rats by Wang *et al.*[3] in 2003. Since then, this imaging modality has been widely researched and advanced toward clinical applications.

The most important chromophores in the human body are oxyhemoglobin and deoxyhemoglobin in red blood cells. The hemoglobins have absorption coefficients of more than 100 cm^{-1} for visible light; hence, they are capable of generating strong photoacoustic signals (~10 bar). Therefore, PAT has been successfully applied to image vascular structures and tumor angiogenesis a few millimeters under the skin.[4−6]

Unlike other high-resolution optical imaging modalities, such as confocal microscopy, two-photon microscopy, and optical coherence tomography, PAT relies on both diffused and ballistic light and thus can be used to image deeper biological tissues. However, because of the overwhelming scattering effect of biological tissues on light, light intensity decreases exponentially with depth with a decay constant that is related to effective penetration depth. The light intensity attenuation can be minimized by choosing an excitation laser wavelength within the near-infrared (NIR) region, in which biological tissues have a relatively low absorption coefficient and a low scattering coefficient.

Wang[7] indicated that the maximum PAT depth was around 50−70 mm, which equaled roughly 10 times the optical effective penetration depth.[6] Oraevsky *et al.*[8] reported a PAT image of a ductal carcinoma at a depth of 1.1 cm below the breast surface and developed a laser PAT system for breast cancer detection at wavelengths of 757 and 1064 nm with an arc-shaped array of 64 acoustic transducers with bandwidth of ~2.5 MHz. Piras *et al.*[9] developed a PAT system using a 1064 nm laser specifically for breast imaging and successfully used this system for breast imaging in a clinical study. The imaging contrast in these studies arose from differences in the intrinsic properties of blood perfusion owing to angiogenesis and hypoxia between normal tissues and

* Address correspondence to cli@mdanderson.org.

Received for review June 22, 2012 and accepted July 19, 2012.

Published online July 19, 2012
10.1021/nn302782y

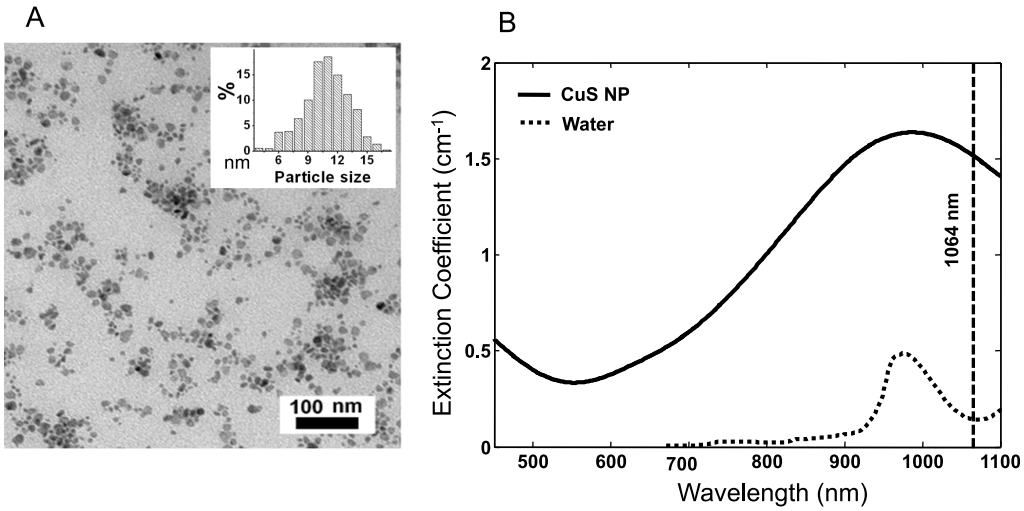

Figure 1. Characterization of CuS NPs. (A) Transmission electron microscopy photograph of CuS NPs. Inset: Size distribution of CuS NPs. (B) Extinction coefficient spectra of 0.5 mM CuS NP aqueous solution (solid line) and pure water (dotted line). The vertical line is positioned at 1064 nm.

tumors. However, these previous approaches to PAT are not applicable for early cancer detection or detection of deeper tumors.

Successful translation of PAT to the clinic requires a practical laser source that efficiently penetrates biological tissues and a contrast agent whose optical absorption peaks at or near the wavelength of the laser source. Among the pulsed lasers available for NIR, the Q-switched Nd:YAG laser, which emits laser light at 1064 nm, is one of the most reliable and economical. However, at 1064 nm, tumor cells have little specific optical absorption that clearly distinguishes them from normal cells. To enhance the optical absorption of tumor cells and to increase the photoacoustic signal-to-noise ratio, it is imperative that exogenous optical contrast agents with strong absorption at 1064 nm be identified and evaluated. Such contrast agents, when selectively delivered to tumor cells, are expected to increase the specificity and sensitivity of the current PAT techniques for early tumor detection. Although several organic dyes and nanoparticles that absorb light in the NIR region of 564 to 824 nm have been evaluated as potential contrast agents for molecular PAT of cancer,[10−14] no contrast agent that absorbs light at 1064 nm has been reported thus far. Here, we report a novel class of semiconductor copper sulfide nanoparticles (CuS NPs) with optical absorption tuned to 990 nm as an excellent PAT contrast agent suitable for deep tissue PAT imaging.

RESULTS AND DISCUSSION

Previously, we demonstrated that CuS NPs exhibit quantum size confinement phenomenon and that the interaction of CuS NPs with 808 nm NIR light can generate heat for photothermal ablation therapy of cancer cells.[15,16] Here, we found that the absorption peak could be tuned toward longer wavelengths by simply adjusting the stoichiometric ratio between $CuCl_2$ and Na_2S. Figure 1A is a transmission electron microscopy photograph of the type of CuS NPs employed in our study. The average diameter of the CuS NP was 11 $\pm$ 3 nm. Figure 1B shows the extinction coefficient spectrum of CuS NP in aqueous solution equivalent to 0.5 mM CuS molecules. The absorption peaked at around 990 nm. At the wavelength of 1064 nm, the CuS NP's extinction measured in a quartz cuvette of a 1.0 cm optical path length was 0.66. Thus, the molar extinction coefficient of CuS molecules was 1.3×10^3 cm^{-1} M^{-1}. Taking the known values of the average diameter of CuS NPs (11 nm) and density (4.76 g/cm^3) and assuming that the scattering signal was negligible, it is estimated that the molar absorption coefficient for CuS NPs at 1064 nm was 2.6×10^7 cm^{-1} M^{-1}. The strong absorption at 1064 nm suggests that CuS NPs are an excellent candidate for contrast enhancement for PAT. A cell viability assay showed that CuS NPs had minimal cytotoxicity at concentrations of up to 96 μg/mL after 24 h incubation (Supplementary Figure 1).

Figure 2 shows *in vivo* PAT images of a mouse brain acquired with green light at 532 nm without contrast agent (Figure 2A) and with NIR light at 1064 nm using CuS NPs as a contrast agent (Figure 2B and C). Hemoglobin is the major chromophore in biological tissues and has strong absorption of green light at the wavelength of 532 nm. Therefore, green light is ideal for imaging of vascular structures. However, green light cannot penetrate deeply because of strong tissue absorption and scattering at short wavelengths. The superficial vascular structures of the mouse brain, such as the veins and arteries in the cerebral and temporal lobes, were clearly visible with green light (Figure 2A). In contrast, on PAT images of the mouse brain acquired at 1064 nm, only the sagittal and transverse sinuses

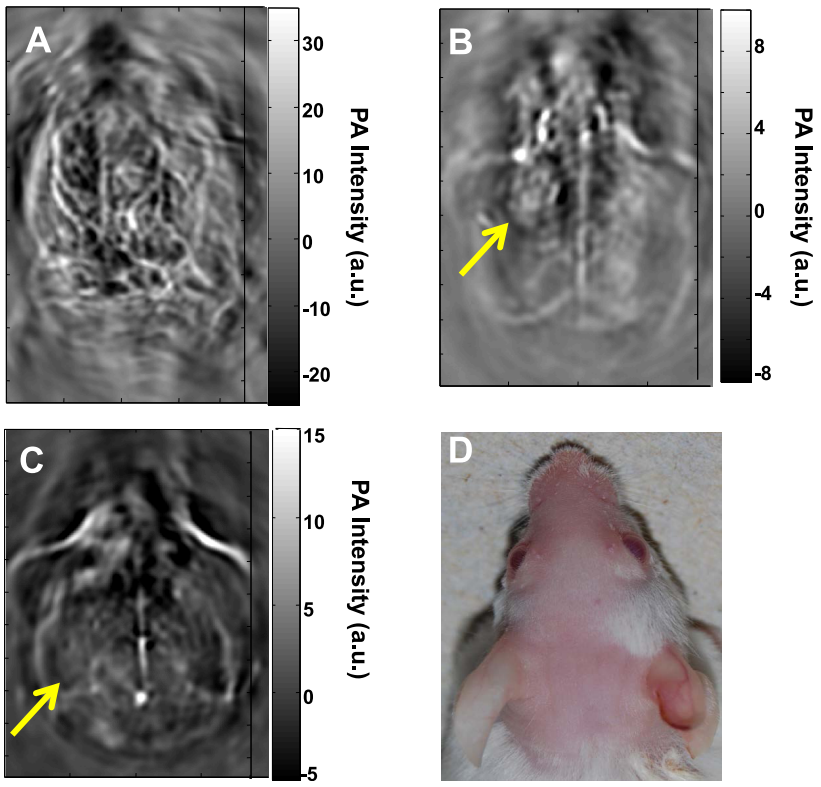

Figure 2. Representative *in vivo* PAT images of a mouse brain. Images were acquired using laser light (A) at a wavelength of 532 nm without contrast agent, (B) at 1064 nm 24 h after intracranial injection of 15 μL of CuS NP solution, and (C) at 1064 nm 7 days after intracranial injection of 15 μL of CuS NP solution. (D) Photograph of the head of the mouse. Laser light was delivered from the top.

were visualized; blood vessels were not discernible (Figure 2B and C). Significantly, a nodule on the left cerebral cortex that was injected intracranially with 15 μL of an aqueous solution of CuS NPs (3×10^{13} NP/mL, 96 μg NP/mL, 2 OD) 24 h before PAT acquisition was clearly delineated (Figure 2B). Seven days after CuS NP injection, the nodule in Figure 2B had dissolved, presumably because CuS NPs had cleared from the injection site to be below the detection limit (Figure 2C).

Figure 3 shows PAT images of the axillary and brachial lymph nodes of a rat 24 h after interstitial injection of CuS NPs into the front paw pad on one side of the body. The lymph nodes, located 12 mm below the skin surface, were clearly visualized (Figure 3A). In contrast, the axillary and brachial lymph nodes on the contralateral side, which did not receive an interstitial injection of CuS NP, were not visualized on PAT (Figure 3C). To ensure that the lymph nodes were within the imaging field of view, stainless steel needle tips were placed adjacent to the targets as a reference (red arrows, Figure 3A and C).

The PAT experiment on detection of axillary and brachial lymph nodes was conducted in three rats. PAT images in all rats depicted uptake of CuS NPs by ipsilateral draining lymph nodes after interstitial injection of the nanoparticles. A representative lymph node PAT image and its one-dimensional photoacoustic signal profile (along the dot-dashed line in Figure 3E) are shown in Figure 3E and F. For quantitative comparison, the absolute photoacoustic signal intensity of each image pixel within the lymph node region of interest from each rat was obtained and used to calculate the mean signal intensity and standard deviation. The photoacoustic signal intensity was significantly higher in lymph nodes containing CuS NPs than in lymph nodes without CuS NPs (7.85 ± 3.78 *vs* 2.46 ± 0.73 au, $p = 0.026$).

To determine the effective PAT imaging depth at a wavelength of 1064 nm, agarose gels containing CuS NPs were embedded in a piece of chicken breast muscle, which was then placed under other pieces of chicken breast muscle, each approximately 1.5 cm thick (Figure 4A). The number of pieces of chicken breast muscle placed on top of the piece with embedded CuS NPs was varied so that the depth below the surface of the piece with embedded CuS NPs varied from 1 to 5 cm. Six agarose gel objects, containing CuS NPs of 100, 50, 25, 12.5, 6.25, and 0 μg/mL, were sequentially embedded counterclockwise starting at the one o'clock direction. Two stainless steel needle tips were placed in the same plane as the agarose gels at the center and 11 o'clock position, respectively, as references. Figure 4C and D show PAT images obtained with the 2.25 MHz transducer when a piece of chicken breast muscle embedded with CuS NPs was placed at depths of 2.5 and 5 cm, respectively. At 2.5 cm, all the

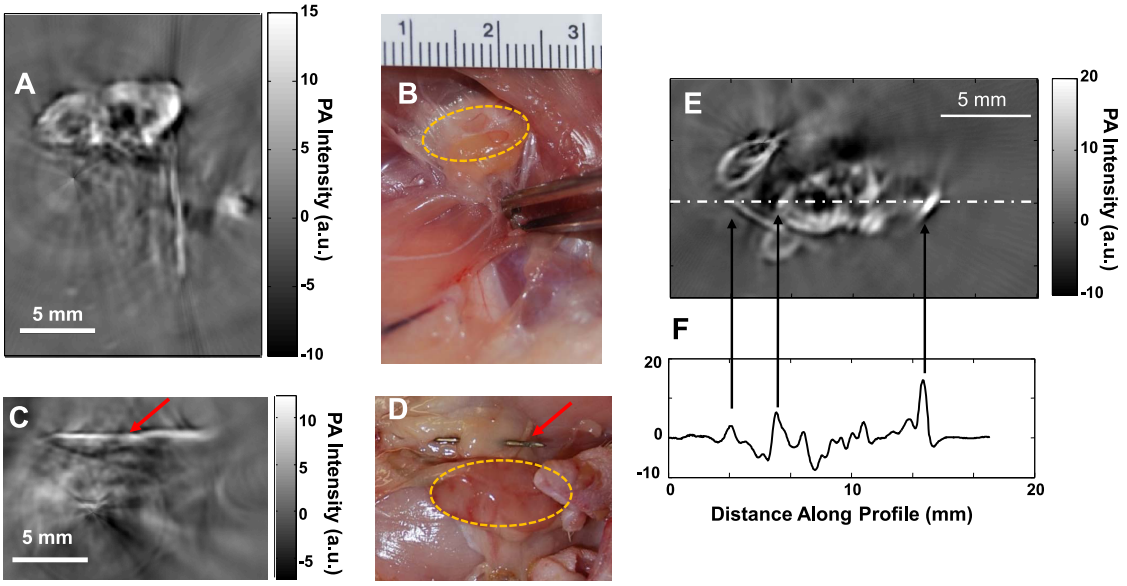

Figure 3. Representative PAT images of axillary and brachial lymph nodes at a depth of 12 mm below the skin of rats. (A, B) PAT image acquired on the right side of a rat 24 h after interstitial injection of 200 μL of CuS NP solution into the right front paw pad (A) and corresponding photograph of exposed rat underarm after imaging experiment (B). (C, D) PAT image acquired on the left side, into which no CuS NPs were injected (C), and corresponding photograph of exposed rat underarm after imaging experiment (D). Yellow circles indicate lymph nodes. Red arrows indicate stainless steel needle tips placed adjacent to the lymph nodes to ensure that they were within the imaging field of view. (E) Representative PAT image of axillary and brachial lymph nodes in a different rat. (F) One-dimensional profile showing PA signal intensity along the dashed line in (E).

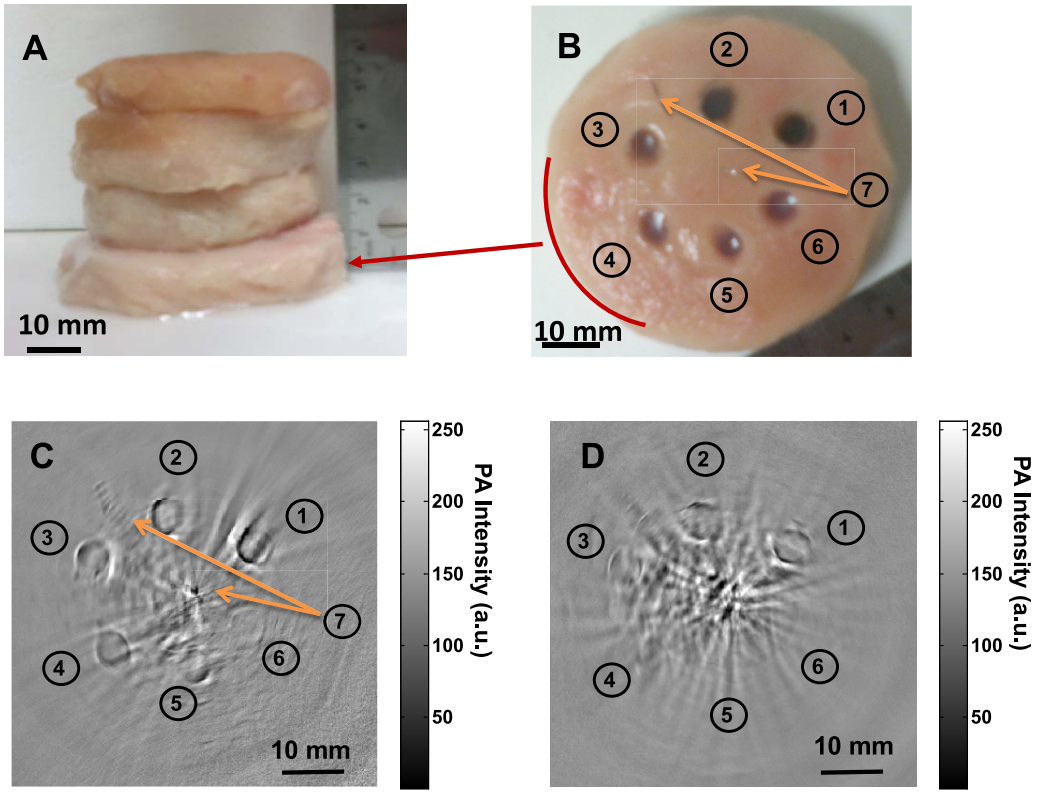

Figure 4. Comparison of deep embedded objects and their photoacoustic images. Agarose gels containing CuS NPs were embedded in a piece of chicken breast muscle, which was then placed under varying numbers of other pieces of chicken breast muscle. Photograph of (A) chicken breast muscle blocks stacked, (B) the cross section of chicken breast muscle where copper sulfide nanoparticles of ① 100 μg/mL (2 OD), ② 50 μg/mL (1 OD), ③ 25 μg/mL (0.5 OD), ④ 12.5 μg/mL (0.25 OD), ⑤ 6.25 μg/mL (0.125 OD), ⑥ gel without contrast agent, and ⑦ two needle tips at center and 11 O'clock position are embedded; two-dimensional photoacoustic image at a depth of (C) ~2.5 cm and (D) ~5 cm, from laser-illuminated surface.

TABLE 1. Effective Attenuation Coefficients and Penetration Depth of 1064 nm Light in Chicken Breast Muscle by Exponential Fitting of Photodiode Signals and Reconstructed Photoacoustic Amplitudes at Various Depths

	effective attenuation coefficient (mm^{-1})	95% confidence interval	R^2	effective penetration depth (mm)
reconstructed needle tip	0.18	(0.10, 0.21)	0.97	5.6
reconstructed CuS NPs of 100 mg/L	0.12	(0.11, 0.13)	0.99	8.3
photodiode signal amplitude	0.17	(0.14, 0.20)	0.98	5.9

agarose gel objects including plain agarose gel without CuS NPs were clearly visualized. These data indicate that CuS NPs enhanced photoacoustic contrast between the agarose gel and chicken breast tissue. The data also indicate that PAT could detect intrinsic differential optical absorbance between the agarose gel and chicken breast tissue at 1064 nm and depths of up to 2.5 cm. At 5 cm, the agarose gel objects containing 100, 50, and 25 μg/mL CuS NPs remained detectable. PAT imaging resolution in the central area is estimated to be approximately 800 μm according to the photoacoustic detection bandwidth.[17] On the basis of the visibility at 25 μg/mL and resolved voxel size of 2.56 mm^3, the imaging sensitivity to CuS NPs at a depth of 5 cm was estimated to be ~0.7 nmol of CuS molecules per image voxel. At a depth of 2.5 cm, the sensitivity to CuS NPs was estimated to be <0.2 nmol of CuS molecules per image voxel.

The minimal detectable concentrations of 6.25 μg/mL at 2.5 cm depth and 25 μg/mL at 5 cm depth are quite high. Whether these concentrations in solid tumors are achievable after systemic injection remains to be seen. Assuming that CuS NPs can be safely injected at a dose of 0.042 mmol CuS/kg (4.0 mg/kg) and that 10% of injected dose is deposited to one gram of tumor, the concentration of CuS NPs in the tumor of a 25 g mouse could reach ~10 μg/g (10 μg/mL). This value is on the same order of magnitude as the minimal detectable concentration of 6.25−25 μg/mL obtained using our prototype photoacoustic imaging device employing a single element transducer. It is expected that by using a more powerful 1064 nm laser and a more sensitive ultrasonic detector array for photoacoustic signal generation and detection, it is possible to significantly increase the detection sensitivity. Therefore, it is feasible to use CuS NPs as the contrast agents in molecular photoacoustic imaging at 1064 nm in an *in vivo* setting.

The optical fluence attenuation in chicken breast at 1064 nm can be calculated using photoacoustic data obtained at different depths. The photoacoustic intensities were derived from the reconstructed images and calibrated by the signal amplifications employed in the experiment. Given the photoacoustic signal intensity generated from stainless steel needle tips and gels containing 100 μg/mL CuS NPs, the effective attenuation coefficients were found to be 0.18 and 0.12 mm^{-1}, respectively, by exponential fitting based on Beer's law. In comparison, the effective attenuation coefficient obtained by measuring light intensities through chicken breast of different thickness using a photodiode detector was 0.17 mm^{-1}. The difference between photoacoustic and photodiode measurements can be partially explained by deviation of light distribution from strict Beer's law. The fitted effective attenuation coefficients, statistical parameters, and estimated effective penetration depths (multiplicative inverse of effective attenuation coefficient) are summarized in Table 1.

The reported optical properties of human breast tissue vary between different studies. Cerussi *et al.*[18] presented the results of a clinical study performed in 58 patients with stage II/III malignant breast tumors using a noninvasive broadband optical spectroscopy probe. They presented the spectra for breast tumors and contralateral normal breast tissues. According to their data extrapolated from 1000 to 1064 nm, the optical penetration depths in normal breast tissues were 11.4 mm at 800 nm and 6.6 mm at 1064 nm. Taroni *et al.*[19] measured *in vivo* absorption and scattering spectra of breast tissue from 10 healthy volunteers at wavelengths between 600 and 1100 nm. The effect of tissue composition on optical properties was evaluated in terms of blood oxygen level and water and lipid content using a spectrally constrained global fitting procedure. The penetration depths at 800 and 1064 nm were estimated to be 7.0 and 5.2 mm, respectively.

The photoacoustic intensities of CuS NP-containing gels at different depths in chicken breast were derived from the reconstructed images and calibrated according to the signal amplifications employed in the experiment. Figure 5 shows the experimental data and its exponential fitting, revealing the attenuation of 1064 nm laser light in chicken breast as a function of depth. For comparison, the light attenuations in human breast are also plotted in Figure 5 using the data from Cerussi *et al.*[18] and Taroni *et al.*[19] The maximum imaging depth of 50 mm achieved in our experiment amounts to approximately 6 times the effective optical penetration depth, corresponding to a 26 dB attenuation of the transmitted light from the surface incident light of 100 mJ/cm^2 to ~0.24 mJ/cm^2. In other words, using an initial light fluence of 100 mJ/cm^2 at a surface as excitation, the CuS NP-containing objects can be imaged at 6 times the effective optical penetration depth. By comparing the effective penetration depths of the chicken breast used in our experiments and

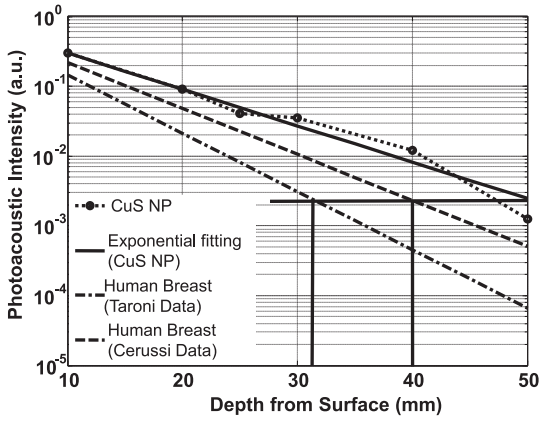

Figure 5. Experimental PA signal intensity of CuS NPs contained in agarose gel embedded in chicken breast muscle measured at a wavelength of 1064 nm as a function of depth from the laser-illuminated surface. Predicted PA intensities of human breast tissue based on historical data are indicated by the dashed line and the dash-dotted line.

human breast tissues, an estimation of the imaging depth in human breast tissue can be made. According to the optical effective penetration depths of 6.6 and 5.2 mm measured by Cerussi *et al.*[18] and Taroni *et al.*,[19] respectively, in human breast tissues, the imaging depths equivalent to 6 times the effective optical penetration depth at 1064 nm would be 40 and 31 mm, respectively, in human breast tissues.

Compared with other NIR lasers, the Q-switched Nd:YAG laser is available at much higher energy level and much lower cost. In fact, its second harmonic radiation at 532 nm is usually employed to pump other laser media, such as Ti:Sapphire, laser dyes, and optical parametric oscillators, to obtain tunable laser output in the NIR region. The laser energy conversion efficiency is characteristically around 10% (~50% for second-harmonic generation and ~20% for pumping other laser media). Typical commercial pulsed Q-switched Nd:YAG laser outputs are ~1 J/pulse at 1064 nm (fundamental oscillation), ~500 mJ/pulse at 532 nm (second harmonic), and ~100 mJ/pulse maximum at 800 nm (pumping Ti:Sapphire laser). With 10 times greater available laser pulse energy, the fluence rate of a 1064 nm laser would be much greater than that of an 800 nm laser at a ≤40 mm depth in human breast. This should translate to a stronger photoacoustic signal and higher signal-to-noise ratio in the region necessary for molecular imaging of breast cancer.

CONCLUSIONS

Employing a low-cost Nd:YAG laser at a wavelength of 1064 nm for photoacoustic excitation, PAT clearly visualized CuS NPs in mouse brain and rat lymph nodes. Moreover, agarose gel containing CuS NPs embedded in chicken breast at a depth of ~5 cm could be readily imaged with an in-plane imaging resolution of ~800 μm and a sensitivity of ~0.7 nmol per imaging voxel. Our study indicates that it should be possible to image lesions in the human breast at a depth of up to 40 mm with imaging resolution and sensitivity similar to that obtained with CuS NPs in chicken breast muscles. In addition to breast, lesions located in other anatomic sites such as skin, arm or leg, head and neck, and lymph nodes may also be detected with the next generation of photoacoustic imaging devices equipped with more powerful 1064 nm lasers and a more sensitive ultrasonic detection array. Future studies, in particular *in vivo* imaging studies of targeted CuS NPs, are warranted to establish the potential utility of the 1064 nm laser in molecular photoacoustic imaging.

METHODS

Materials. Copper(II) chloride ($CuCl_2$), sodium sulfide ($Na_2S \cdot 9H_2O$), sodium citrate, and methoxy-PEG-thiol (PEG-SH, molecular weight 5000) were purchased from Sigma-Aldrich (St. Louis, MO, USA). Isoflurane was purchased from Baxter (Deerfield, IL, USA).

General Procedure for the Synthesis of CuS NPs. Into 1000 mL of an aqueous solution of $CuCl_2$ (1 mmol) and sodium citrate (0.68 mmol) was added 1 mL of sodium sulfide solution (Na_2S, 1 M) under stirring at room temperature. Five minutes later, the reaction mixture was heated to 90 °C and stirred at 1000 rpm for 15 min until a dark green solution was obtained. Nanoparticles with peak absorption at 990 nm were obtained by adjusting the stoichiometric ratio between $CuCl_2$ and Na_2S. To introduce a PEG coating, about 1 mg of PEG-SH was added into the citrate–CuS NP solution (3.0×10^{13} NP/mL water, 0.096 mg/mL, 2 OD at 1064 nm). The reaction was allowed to proceed overnight at room temperature.

Characterization of CuS NPs. For transmission electron microscopy, an aqueous solution of CuS NPs was deposited on carbon-enhanced copper grids without negative staining. The NPs were allowed to adhere on the grid for 1 h, after which they were briefly rinsed with deionized water and air-dried. The samples were then examined using a transmission electron microscope (JEM 2010, JEOL Japan) at an accelerating voltage of 200 kV. Digital images were obtained using the AMT Imaging System (Advanced Microscopy Techniques Corp., Danvers, MA, USA). The average diameter of the CuS NPs was determined by measuring up to 200 individual particles. The extinction spectrum of the nanoparticles was measured using a UV–vis spectrophotometer (DU 800, Beckman Coulter, Inc., Brea, CA, USA). The fraction of incident light transmitted through a solution of nanoparticles was recorded, and then the extinction coefficient was derived according to energy conservation.

PAT Imaging Equipment. Our PAT experimental setup is shown in Supplementary Figure 2. A Q-switched Nd:YAG laser (LS-2137, Symphotic Tii, Camarillo, CA, USA) provides 15 ns, ~1000 mJ NIR and ~500 mJ green laser pulses at wavelengths of 1064 and 532 nm, respectively, at a repetition rate of 10 Hz. The laser beam is expanded by a concave lens and homogenized by a ground glass lens and then directed onto a test sample, *e.g.*, rat head, rat underarm, or the sample made from chicken breast muscle. The incident laser energy density on the tissue surface is controlled at ~100 or ~20 mJ/cm^2, which are the "maximum permissible exposure" for human skin at the pulse width and wavelength of 1064 and 532 nm, respectively. NIR light diffuses inside a tissue sample and induces photoacoustic waves.

The waves travel through the tissue and are coupled to the ultrasonic transducer, which converts the photoacoustic pressure into piezoelectric signals. An unfocused ultrasonic transducer (V323/2.25 MHz, Panametrics, Waltham, MA, USA) with a 6 mm diameter active element and 1.8 MHz detection bandwidth is employed to receive photoacoustic waves. The signals are subsequently amplified by amplifiers (ZFL-500LN, Mini-Circuits and 5072PR, Panametrics, Waltham, MA, USA), bandpass-filtered by our homemade filters, and finally recorded using a digital data acquisition card (CS14100, Gage Applied, Inc., Lockport, IL, USA). The sample and transducers are both immersed in a tank filled with saline for coupling the photoacoustic waves to the transducers. The ultrasonic transducer is driven by a step motor to continuously scan horizontally along a 15 cm diameter circle around the sample. A personal computer is used to control the scanning and data acquisition.

Imaging Mouse Brain and Sentinel Lymph Nodes in Rats. All experiments involving animals were done in accordance with the guidelines of the Institutional Animal Care and Use Committee. For the *in vivo* photoacoustic imaging experiment on mouse brain, three mice (Charles River Laboratories, Wilmington, MA, USA) weighing ~25 g were anesthetized using veterinary anesthesia equipment (Mobile 901807, VetEquip, Pleasanton, CA, USA) that delivered 2% isoflurane in oxygen at a flow rate of 2 L/min. The hairs on each mouse's head were gently removed by applying hair-remover lotion. Laser light was used to illuminate the animal head from its top, and an ultrasonic detector was used to scan the animal's head in its horizontal plane. CuS NPs (3×10^{13} NP/mL, 0.096 mg/mL, 2 OD at 1064 nm) in 15 μL of saline were injected intracranially into the left cerebral cortex of each mouse ($n = 3$) at a depth of ~2 mm beneath the mouse skull.

For the *ex vivo* photoacoustic imaging experiment on rat lymph nodes, five Sprague–Dawley rats (Charles River Laboratories) weighing 250–300 g received subcutaneous injections of 1 mg/site of CpG oligodeoxynucleotides (Alpha NDA 365217, Montreal, Quebec, Canada) 24 h before the injection of CuS NPs (0.096 mg/mL, 300 μL) *via* the right front paw pad. Twenty-four hours after nanoparticle injection, the animals were euthanized, and PAT imaging experiments were performed.

Imaging Gel Embedded in Chicken Breast Tissues. To determine maximum imaging depth, various gel cylinders (5 mm in diameter × 4 mm in length) were embedded in chicken breast muscles of ~9 cm in diameter. Six gel objects were obtained by mixing 2% agarose with CuS NPs at concentrations of 100, 50, 25, 12.5, 6.25, and 0 μg/mL. Two stainless steel needle tips were also placed in the same plane as a reference. When excited by laser light from the top, the embedded objects emit photoacoustic waves when they absorb the light energy. The photoacoustic signals were detected by the circularly scanning transducers and fed into the image reconstruction on the basis of a back-projection algorithm. The tissue's cross-section containing the embedded objects was imaged when blocks of chicken breast muscles were sequentially stacked to make the embedded objects at the desired depths from the laser-illuminated tissue surface. The light intensities that transmitted through various tissue depths were detected using a photodiode detector (DET110, Thorlabs, Newton, NJ, USA).

Conflict of Interest: The authors declare no competing financial interest.

Acknowledgment. The authors thank Stephanie Deming for editing the manuscript. We also thank K. Dunner for assistance with the transmission electron microscopy facility. This work was supported in part by National Cancer Institute grant R01CA119387-05S1, a Seed Grant through the Alliance for NanoHealth by the Department of Army Telemedicine and Advanced Technology Research Center (W81XWH-07-2-0101), and the John S. Dunn Foundation. The University of Texas MD Anderson Cancer Center is supported in part by the National Institutes of Health through Cancer Center Support Grant CA016672.

Supporting Information Available: Cytotoxicity of CuS NPs; description and scheme of photoacoustic setup. This material is available free of charge *via* the Internet at http://pubs.acs.org.

REFERENCES AND NOTES

1. Kruger, R. A. Photoacoustic Ultrasound. *Med. Phys.* **1994**, *21*, 127–131.
2. Oraevsky, A. A.; Jacques, S. L.; Tittel, F. K. Measurement of Tissue Optical Properties by Time-Resolved Detection of Laser-Induced Transient Stress. *Appl. Opt.* **1997**, *36*, 402–415.
3. Wang, X. D.; Pang, Y. J.; Ku, G.; Xie, X. Y.; Stoica, G.; Wang, L. H. V. Noninvasive Laser-Induced Photoacoustic Tomography for Structural and Functional *in Vivo* Imaging of the Brain. *Nat. Biotechnol.* **2003**, *21*, 803–806.
4. Jose, J.; Manohar, S.; Kolkman, R. G. M.; Steenbergen, W.; van Leeuwen, T. G. Imaging of Tumor Vasculature Using Twente Photoacoustic Systems. *J Biophotonics* **2009**, *2*, 701–717.
5. Kolkman, R. G. M.; Hondebrink, E.; Steenbergen, W.; de Mul, F. F. M. *In Vivo* Photoacoustic Imaging of Blood Vessels Using an Extreme-Narrow Aperture Sensor. *IEEE J. Sel. Top. Quant.* **2003**, *9*, 343–346.
6. Ku, G.; Wang, X. D.; Xie, X. Y.; Stoica, G.; Wang, L. H. V. Imaging of Tumor Angiogenesis in Rat Brains *in Vivo* by Photoacoustic Tomography. *Appl. Opt.* **2005**, *44*, 770–775.
7. Wang, L. V. Prospects of Photoacoustic Tomography. *Med. Phys.* **2008**, *35*, 5758–5767.
8. Oraevsky, A. A.; Ermilov, S. A.; Conjusteau, A.; Miller, T.; Gharieb, R. R.; Lacewell, R.; Mehta, K.; Radulescu, E. G.; Herzog, D.; Thompson, S. T.; *et al*. Initial Clinical Evaluation of Laser Optoacoustic Imaging System for Diagnostic Imaging of Breast Cancer. *Breast Cancer Res. Treat.* **2007**, *106*, S47–S47.
9. Piras, D.; Xia, W. F.; Steenbergen, W.; van Leeuwen, T. G.; Manohar, S. Photoacoustic Imaging of the Breast Using the Twente Photoacoustic Mammoscope: Present Status and Future Perspectives. *IEEE J. Sel. Top. Quant. Electron.* **2010**, *16*, 730–739.
10. Kim, C.; Cho, E. C.; Chen, J.; Song, K. H.; Au, L.; Favazza, C.; Zhang, Q.; Cobley, C. M.; Gao, F.; Xia, Y.; *et al*. *In Vivo* Molecular Photoacoustic Tomography of Melanomas Targeted by Bioconjugated Gold Nanocages. *ACS Nano* **2010**, *4*, 4559–4564.
11. De la Zerda, A.; Zavaleta, C.; Keren, S.; Vaithilingam, S.; Bodapati, S.; Liu, Z.; Levi, J.; Smith, B. R.; Ma, T. J.; Oralkan, O.; *et al*. Carbon Nanotubes As Photoacoustic Molecular Imaging Agents in Living Mice. *Nat. Nanotechnol.* **2008**, *3*, 557–562.
12. Lu, W.; Melancon, M. P.; Xiong, C.; Huang, Q.; Elliott, A.; Song, S.; Zhang, R.; Flores, L. G.; Gelovani, J. G.; Wang, L. V.; *et al*. Effects of Photoacoustic Imaging and Photothermal Ablation Therapy Mediated by Targeted Hollow Gold Nanospheres in an Orthotopic Mouse Xenograft Model of Glioma. *Cancer Res.* **2011**, *71*, 6116–6121.
13. Pan, D.; Pramanik, M.; Senpan, A.; Yang, X.; Song, K. H.; Scott, M. J.; Zhang, H.; Gaffney, P. J.; Wickline, S. A.; Wang, L. V.; *et al*. Molecular Photoacoustic Tomography with Colloidal Nanobeacons. *Angew. Chem., Int. Ed.* **2009**, *48*, 4170–4173.
14. Li, M. L.; Oh, J. T.; Xie, X. Y.; Ku, G.; Wang, W.; Li, C.; Lungu, G.; Stoica, G.; Wang, L. V. Simultaneous Molecular and Hypoxia Imaging of Brain Tumors *in Vivo* Using Spectroscopic Photoacoustic Tomography. *Proc. IEEE* **2008**, *96*, 481–489.
15. Li, Y. B.; Lu, W.; Huang, Q.; Huang, M.; Li, C.; Chen, W. Copper Sulfide Nanoparticles for Photothermal Ablation of Tumor Cells. *Nanomedicine* **2010**, *5*, 1161–1171.
16. Zhou, M.; Zhang, R.; Huang, M.; Lu, W.; Song, S.; Melancon, M. P.; Tian, M.; Liang, D.; Li, C. A Chelator-Free Multifunctional [64Cu]CuS Nanoparticle Platform for Simultaneous Micro-PET/CT Imaging and Photothermal Ablation Therapy. *J. Am. Chem. Soc.* **2010**, *132*, 15351–11358.

17. Ku, G.; Wang, X.; Stoica, G.; Wang, L. V. Multiple-Bandwidth Photoacoustic Tomography. *Phys. Med. Biol.* **2004**, *49*, 1329–1338.
18. Cerussi, A.; Shah, N.; Hsiang, D.; Durkin, A.; Butler, J.; Tromberg, B. J. *In Vivo* Absorption, Scattering, and Physiologic Properties of 58 Malignant Breast Tumors Determined by Broadband Diffuse Optical Spectroscopy. *J. Biomed. Opt.* **2006**, *11*, 044005–044005.
19. Taroni, P.; Bassi, A.; Comelli, D.; Farina, A.; Cubeddu, R.; Pifferi, A. Diffuse Optical Spectroscopy of Breast Tissue Extended to 1100 nm. *J. Biomed. Opt.* **2009**, *14*, 054030–054030.